

Quench Margin Measurement in Nb₃Sn Quadrupole Magnet

V. V. Kashikhin, R. Bossert, G. Chlachidze, M. Lamm, I. Novitski, and A. V. Zlobin

Abstract—One of the possible practical applications of the Nb₃Sn accelerator magnets is the LHC luminosity upgrade that involves replacing the present NbTi focusing quadrupoles in two high-luminosity interaction regions (IR). The IR magnets are exposed to strong radiation from the interaction point that requires a detailed investigation of the magnet operating margins under the expected radiation-induced heat depositions. This paper presents the results of simulation and measurement of quench limits and temperature margins for a Nb₃Sn model magnet using a special midplane strip heater.

Index Terms—Stability, superconducting accelerator magnets, quench limit, temperature margin, thermal modeling.

I. INTRODUCTION

FERMILAB in collaboration with other U.S. laboratories is working on the development of Nb₃Sn magnet technology for particle accelerators. One of the possible practical applications of the Nb₃Sn accelerator magnets is the LHC luminosity upgrade that involves replacing the present NbTi focusing quadrupoles in two high-luminosity IRs [1]. Several Nb₃Sn quadrupole models are being built and tested within the framework of US-LHC Accelerator Research Program (LARP) in order to address the technological challenges and evaluate the performance characteristics.

In addition to high mechanical stresses, the IR magnets are exposed to strong radiation from the interaction point [2]-[3] that warrants an investigation of the magnet operating margins under the expected radiation-induced heat depositions. The radiation heat depositions from the IP are concentrated in the coil midplanes and decay rapidly in both the radial and azimuthal directions [4]. Analysis shows that the maximum temperature also occurs in the coil midplane.

Operating margin of the original NbTi LHC IR quadrupoles was calculated with the help of finite-element codes and measured using a special quadrupole model with high cable AC losses to simulate the radiation heat deposition [5]. A preliminary estimation of the operating margin was also done for Nb₃Sn magnets [6]-[7] using a finite element model with constant thermal properties of magnet structural materials and without experimental verification of the obtained results.

Manuscript received 19 August 2008. This work was supported by the U.S. Department of Energy.

V. V. Kashikhin, R. Bossert, G. Chlachidze, M. Lamm, I. Novitski, and A. V. Zlobin are with the Fermi National Accelerator Laboratory, Batavia, IL 60510 USA (phone: 630-840-6546; fax: 630-840-3369; e-mail: vadim@fnal.gov).

The cables used in Nb₃Sn magnets are insulated by either ceramic or S-2 glass tapes or sleeves of different thicknesses. After winding and high-temperature reaction, the coils are impregnated with epoxy resin. Thus, the fractions of insulation and epoxy in the final coil depend on the type of insulation and the pressures during reaction and impregnation that may vary from magnet to magnet, raising large uncertainties in magnet quench limit under the heat depositions in the coil.

For these reasons, it is important to verify the thermal calculations by the appropriate magnet tests. One of the LARP technological quadrupole models (TQC02b) was equipped with a special strip heater to perform the experimental studies of operating margin in Nb₃Sn quadrupole [8]. The stainless-steel heater was placed in the inner layer midplane, between the adjacent coils made of MJR strand, at the location where the radiation-induced heat depositions exhibit the maximum.

II. THERMAL SIMULATIONS

A. Model Description

The temperature distribution inside the Nb₃Sn quadrupole coil was simulated using COMSOL Multiphysics[®] code. The thermal model included all the details of TQC coil cross-section with the corresponding insulation [9]. The coil had the following types of insulation impregnated with epoxy:

- 0.127-mm of S-2 glass at the inner coil surface, around the cables and the wedges, between the poles and the pole turns;
 - 0.254-mm of S-2 glass between the layers;
 - 0.127-mm of Kapton (polyimide) trace around the coil;
 - 0.127-mm of S-2 glass around the trace;
- The ground insulation consisted of:
- 2x0.127-mm of Kapton around the impregnated coils;
 - 0.533-mm of Kapton between the adjacent coil midplanes.

The 0.025-mm x 9.5-mm stainless steel strip heater was placed in the middle of the Kapton shim package at the coil inner layer. The coil was surrounded by the stainless steel collar and the iron yoke with the outer radius of 200 mm.

Temperature dependencies of thermal properties for all materials were also taken into account in this analysis. The thermal conductivities of copper, bronze, stainless steel, low carbon steel, and insulation were parameterized by analytical functions after [10]-[11]. The thermal properties of epoxy-impregnated S-2 glass insulation were approximated by the properties of a fiberglass composite (G10). Fig. 1 shows the thermal conductivity of insulation materials used in the analysis at low temperatures.

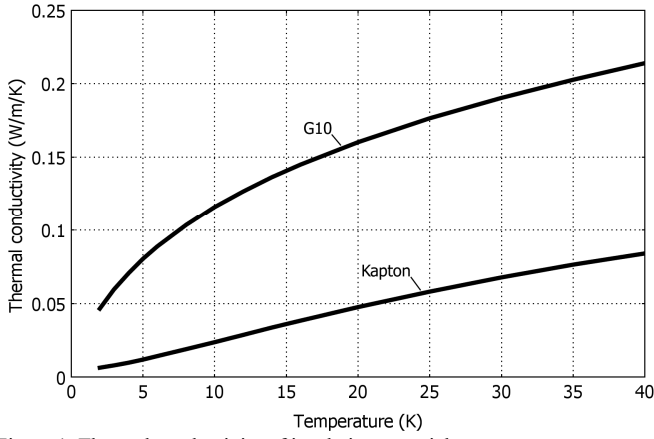


Figure 1. Thermal conductivity of insulation materials.

The boundary conditions included the fixed helium bath temperature T_0 at the inner coil surface and at the outer yoke surface, which are both in direct contact with liquid helium. It was also assumed that the thermal contact resistances between different materials and between the coil and liquid helium are negligibly small.

B. Coil Temperature Profiles

The coil temperature profiles were calculated at T_0 equal to 4.5 K and 1.9 K. An example of the temperature distribution inside the coil heated by the inner-layer midplane strip heater is shown in Fig. 2. Since the thermal conductivity of insulation is at least a factor of thousand lower than that of the metal parts, any conceivable variation of the metal properties (for instance due to different heat treatment conditions, Cu to non-Cu ratios or chemical compositions) have a negligible effect on the temperature profile, and the temperature of each cable is virtually uniform.

As expected, the inner-layer midplane turn, adjacent to the heater, has the maximum temperature. The coil temperature decays quickly in the azimuthal direction, as shown in Fig. 3, due to the efficient heat transfer to liquid helium in the coil aperture and outside of the iron yoke. This decay is more rapid than in the case of the radiation heat depositions [7]. In addition, the midplane temperature of the outer layer, in this case, is lower than that of the inner layer. It explains by different distributions of heat depositions in these two cases.

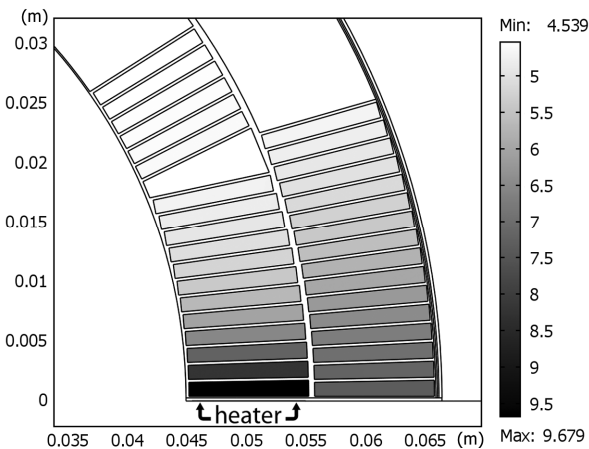


Figure 2. Temperature distribution inside the cable at the heater power of 20 W/m and $T_0 = 4.5$ K.

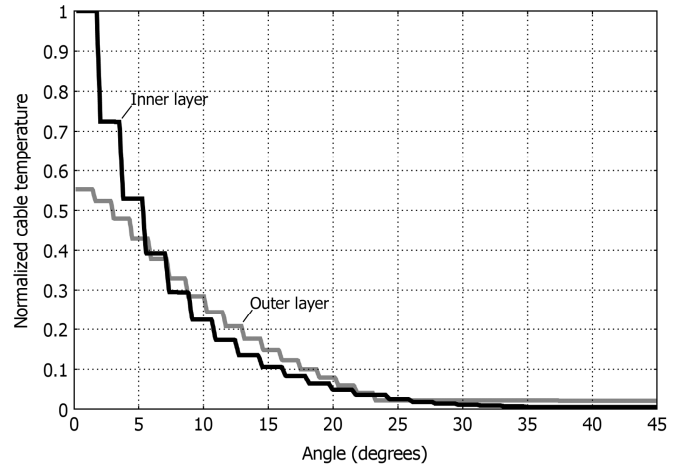


Figure 3. Calculated azimuthal distribution of the temperature increment in the inner and outer layers, normalized by the peak cable temperature.

C. Surface Heat Flux

Fig. 4 shows the peak temperatures of the coil (inner-layer midplane turn) and the heater for different heater power inputs. The electrical resistivity of type 316 stainless steel used for the strip heater is constant up to ~ 50 K. Therefore, the heater power is proportional to the square of the heater current up to ~ 100 W/m that allows using a simple two-wire technique to measure the heater power.

As follows from Fig. 4, less than 70 W/m of heater power is necessary to reach the Nb_3Sn superconductor critical temperature. However, the heat flux from the coil to the liquid helium is relatively high, as shown in Fig. 5, because of the local power concentration in the coil midplane.

The heat flux into helium through the narrow edge of the inner-layer midplane cable reaches 5000 W/m^2 at the heater power of 50 W/m. Experimental data for the He I indicate that the nucleate boiling is preserved for the heat flows up to 6000 W/m^2 at an open surface with the helium temperature rise near the surface less than 0.6 K [12]. After that, film boiling starts with a drastic temperature jump on the coil surface. The estimated critical heat flux to He II is at least a factor of two higher than to He I for the relevant cooling channel.

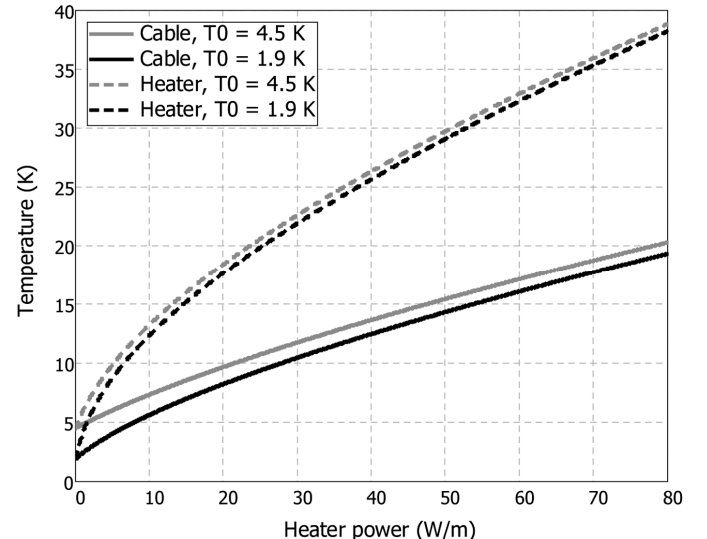


Figure 4. Calculated peak heater and coil temperatures as functions of the heater power.

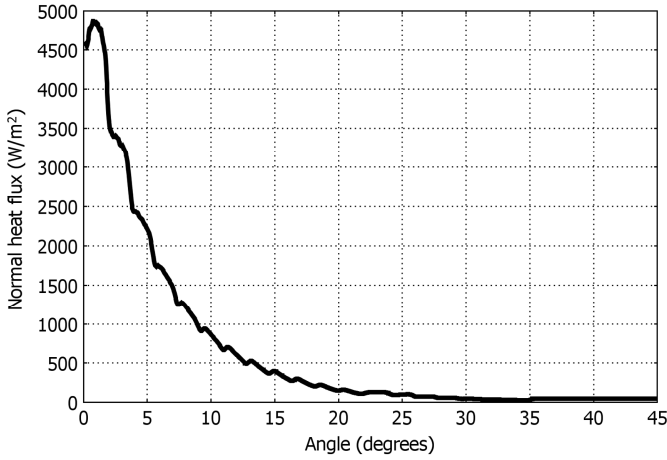


Figure 5. Calculated heat flux to the liquid helium at the inner coil surface, corresponding to the heater power of 50 W/m.

D. Transient Characteristic

For the proper experiment timing, it is important to estimate the thermal diffusion time after powering the heater. The transient analysis was performed on the same model, assuming that the full power is instantaneously delivered to the heater.

The analysis indicated that the inner midplane cable starts heating after 0.001 s of switching on the heater and reaches thermal equilibrium after 10 s. Although the outer pole cable (the most thermally remote spot) temperature is slowly rising even after 100 s, it is of no concern for the given experiment.

E. Load Lines and Temperature Margins

The critical surface of Nb₃Sn cable $I_c(B, T)$ used in TQC02b model was parameterized according to [13] with a low-field correction based on magnetization measurements [14]. No stress/strain correction was applied to either the upper critical field or the critical temperature. The reference critical current density, measured on the corresponding extracted MJR strands, was $J_c(12T, 4.2K) = 1960 \text{ A/mm}^2$. Fig. 6 shows the load lines of the pole and midplane turns of the inner layer along with the critical current curves at different temperatures. The TQC02b short sample limit (SSL) is 12.75 kA and 13.98 kA at 4.5 K and 1.9 K respectively. The temperature margin of the inner-layer midplane cable, calculated from Fig. 6, is presented in Fig. 7. One can see that at 80% of the SSL, the temperature margin is 4-6 K, depending on the T_0 .

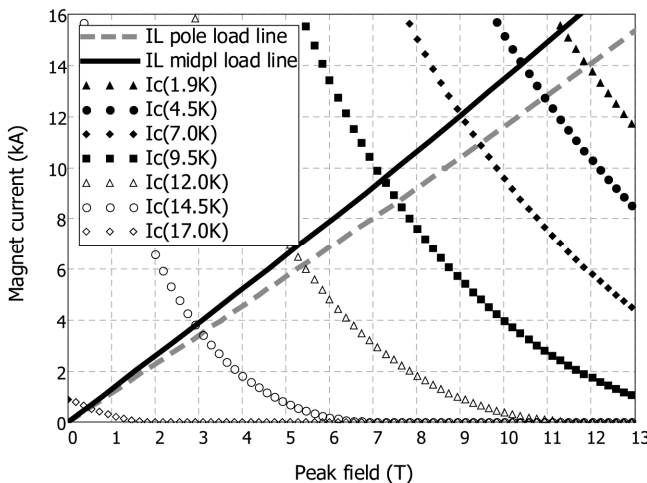


Figure 6. TQC load lines and turn critical currents at different temperatures.

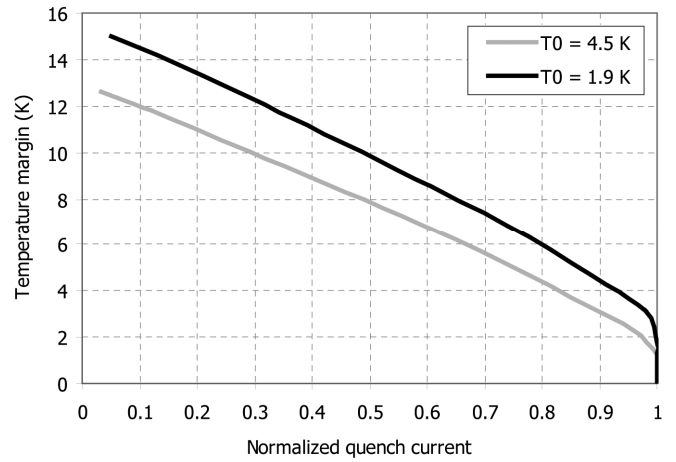


Figure 7. Temperature margin of the midplane cable in the Nb₃Sn quadrupole.

III. MEASUREMENT RESULTS AND DISCUSSION

The heater experiments were performed in TQC02b magnet at 4.5 K and 1.9 K. Each measurement involved setting the heater current to a specific value, and then raising the magnet current to quench with a low ramp rate of 20 A/s to avoid additional coil heating by eddy currents.

Fig. 8 presents the calculated and measured quench currents of the inner midplane cable along with the expected magnet SSL, determined by the inner-layer pole turns. Note that the SSL quoted in this paper does not account for the field enhancement in the coil ends - a specific feature of TQC models due to technological reasons [8].

The calculated quench performance is nearly linear in the whole data range. There is a surprisingly good correlation between the calculated and measured quench currents at 1.9 K, given the assumptions on the insulation thermal properties and boundary conditions. The quench currents measured at 4.5 K are lower than the calculated values and exhibit a non-linear characteristic. The discrepancy at 4.5 K varies from 7% at the heater power of 20 W/m to more than a factor of two at 45 W/m. The observed non-linear behavior is consistent with the increasing heat flux to the helium bath and indicates that there likely is a localized film boiling at the high power inputs that reduces the cooling efficiency of the midplane cables.

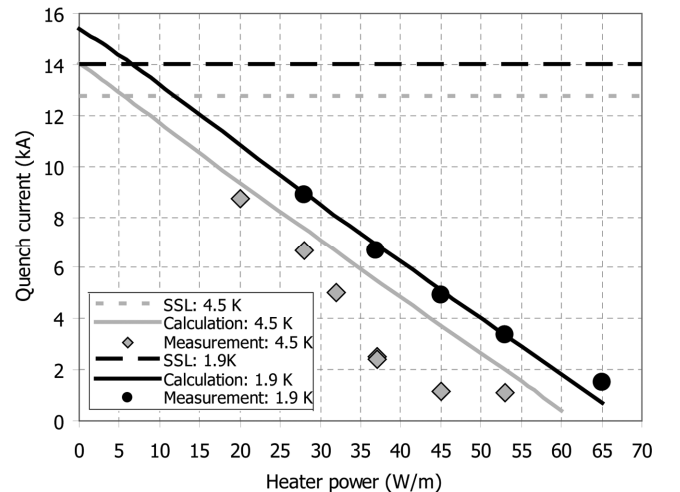


Figure 8. Calculated and measured quench currents as functions of the heater power and the expected short sample limits.

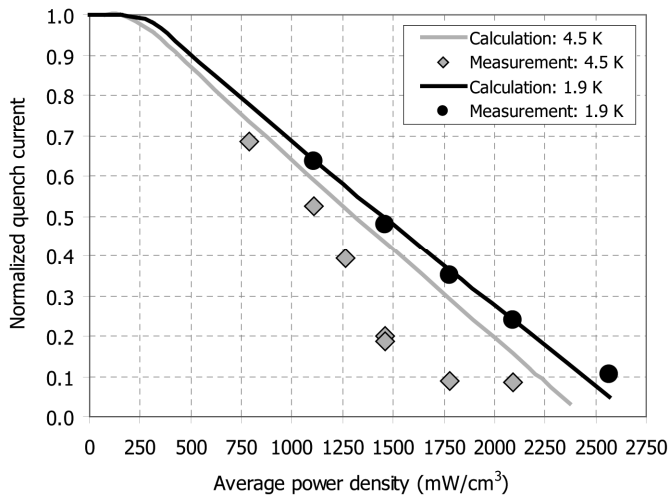


Figure 9. Calculated and measured normalized quench currents as functions of average power density distributed in the midplane cable of inner layer.

Fig. 9 shows the normalized quench current of the inner-layer midplane turn as a function of the average power density of the heat flux in that cable. This plot is essentially invariant with respect to the cable reference critical current density and is valid for any Nb₃Sn conductor used in TQC models. Yet, it is strongly dependent on the particular coil design, heat generation, and cooling schemes.

The good correlation of the measured and calculated data at 1.9 K for the power densities up to 2.2 W/cm³ as well as at 4.5 K for the power densities below 1.2 W/cm³ suggests that the assumptions used in the thermal model are generally correct. The thermal properties of the epoxy-impregnated S-2 glass insulation can be well approximated by the thermal properties of G10 in the temperature range of the Nb₃Sn conductor. The non-linearity observed in the measured quench current at 4.5 K indicates that the heat transfer coefficient from coil to He I becomes important at the heat depositions above 1.2 W/cm³ (heater power above 30 W/m).

The quench limit of Nb₃Sn quadrupoles under the radiation-induced heat depositions from the LHC interaction regions was estimated using the experimentally verified thermal model. The level and details of the radiation heat distribution in the IR quadrupole coils are not fully established yet. The estimate was done for the radiation heat distribution used in [6]-[7].

The preliminary analysis shows that TQC models operating at 80% of their SSL can tolerate 165-185 mW/cm³ of average radiation heat in the inner-layer midplane cables at 4.5 K and 1.9 K respectively. Note that these numbers are smaller than the corresponding values in Fig. 9 due to the previously mentioned different heat distributions in the cases of the midplane heater and radiation-induced heat depositions.

The previous analysis [7] put a quench limit of 42 mW/cm³ for Nb₃Sn IR quadrupoles operating at 1.9 K and 80% of their SSL. It is more than a factor of four lower than the values quoted above. The higher quench limits calculated for the TQC model are explained by a factor of two thinner cable insulation used in that magnet, and by employing the real temperature dependencies of material properties in the thermal model.

IV. CONCLUSION

Simulations and measurements of quench limits at different operating currents and temperatures were performed for the LARP Nb₃Sn quadrupole model of TQC series equipped with a dedicated midplane strip heater. These measurements are the first attempt to experimentally evaluate the quench limits of a Nb₃Sn magnet under artificially-induced heat depositions in the coil midplane.

The calculated and measured data are in a good agreement, verifying the model accuracy, material properties, and boundary cooling conditions. It establishes the confidence in the ability of accurate thermal simulations of magnet performance for different types of Nb₃Sn conductor exposed to various thermal environments (AC losses, radiation heat depositions, etc.).

The level of critical heat depositions (quench limits) in the inner-layer midplane cable is higher than that previously estimated for the Nb₃Sn IR quadrupoles. This result is due to the more realistic, experimentally verified assumptions, used in the present thermal model. The studies of Nb₃Sn magnet quench limits will continue using refined distributions of radiation heat depositions, material properties, and updated magnet designs.

REFERENCES

- [1] J. B. Strait et al., "Towards a New LHC Interaction Region Design for a Luminosity Upgrade," in *Proc. 2003 Particle Accel. Conf.*, pp. 42-44.
- [2] N. V. Mokhov, I. L. Rakhno, J. S. Kerby, and J. B. Strait, "Mitigation of Effects of Beam-Induced Energy Deposition in the LHC High-Luminosity Interaction Regions," in *Proc. 2003 Particle Accel. Conf.*, pp. 1745-1747.
- [3] E. Wildner et al., "Energy Deposited in the High Luminosity Inner Triplets of the LHC by Collision Debris," in *Proc. 2008 European Particle Accel. Conf.*, Genoa, Italy, pp. 2587-2589.
- [4] N. V. Mokhov, I. L. Rakhno, "Mitigating Radiation Loads in Nb₃Sn Quadrupoles for the CERN Large Hadron Collider Upgrades," *Phys. Rev. Special Topics - Accelerators and Beams* 9, 101001 (2006).
- [5] L. Chiesa et al., "Thermal Studies of a High Gradient Quadrupole Magnet Cooled with Pressurized, Stagnant Superfluid," *IEEE Trans. Appl. Supercond.*, vol. 11, no. 1, Mar. 2001, pp. 1625-1628.
- [6] A. V. Zlobin et al., "Large-Aperture Nb₃Sn Quadrupoles for 2nd generation LHC IRs," in *Proc. 2002 European Particle Accel. Conf.*, Paris, France, pp. 2451-2453.
- [7] I. Novitski, A. V. Zlobin, "Thermal Analysis of SC Quadrupoles in Accelerator Interaction Regions," *IEEE Trans. Appl. Supercond.*, vol. 17, no. 2, Jun. 2007, pp. 1059-1062.
- [8] R. C. Bossert et al., "Fabrication and Test of LARP Technological Quadrupole Models of TQC Series," *IEEE Trans. Appl. Supercond.*, vol. 19, no. 3, Jun. 2009.
- [9] R. C. Bossert et al., "Development of TQC01, a 90 mm Nb₃Sn Model Quadrupole for LHC Upgrade Based on SS Collar," *IEEE Trans. Appl. Supercond.*, vol. 16, no. 2, Jun. 2006, pp. 370-373.
- [10] E. D. Marquardt, J. P. Le, R. Radebaugh, "Cryogenic Material Properties Database," in *Proc. 11th Int. Cryocooler Conf.*, Jun. 2000, Keystone, Colorado.
- [11] J. E. Jensen, W. A. Tuttle, R. B. Stewart, H. Brechna, and A. G. Prodel, *Brookhaven National Laboratory Selected Cryogenic Data Notebook*, BNL 10200-R, vol. I, 1980.
- [12] M. N. Wilson, *Superconducting magnets*, Clarendon Press, Oxford, 1983.
- [13] L. T. Summers, M. W. Guinan, J. R. Miller, and P. A. Hahn, "A model for the prediction of Nb₃Sn critical current as a function of field, temperature, strain, and radiation damage," *IEEE Trans. Magn.*, vol. 27, no. 2, Mar. 1991, pp. 2041-2044.
- [14] E. Barzi et al., "Round and Extracted Nb₃Sn Strand Tests for LARP Magnet R&D," *IEEE Trans. Appl. Supercond.*, vol. 16, no. 2, Jun. 2006, pp. 319-323.